# Determination of Solubilities of $CO_2$ in Linear and Branched Polypropylene Using a Magnetic Suspension Balance and a *PVT* Apparatus

**Mohammad M. Hasan,[†] Yao G. Li,[†] Guangming Li,[†] Chul B. Park,*[,†] and Pu Chen[‡]**

Department of Mechanical and Industrial Engineering, University of Toronto, 5 King's College Road, Toronto, Ontario, Canada M5S 3G8, and Department of Chemical Engineering, University of Waterloo, 200 University Avenue West Waterloo, Ontario, Canada N2L 3G1

Using a *PVT* apparatus for high pressure and temperature combined with a magnetic suspension balance, the solubility of carbon dioxide in linear and branched polypropylene (PP) was measured at temperatures from (453 to 493) K and at pressures of up to 31 MPa. The solubility of $CO_2$ in both molten polymers increased linearly with pressure and decreased with temperature. However, above 20 MPa, the solubility−pressure relationship was no longer linear. This might be due to a significant hydrostatic effect on the swelling of the polymer that results from gas absorption above 20 MPa, so that swelling is no longer linearly related to pressure. At a high pressure, swelling significantly affects solubility, which is then no longer linearly related to pressure. It was noted that linear PP absorbs more gas than branched PP, due to the branched PP's chain entanglement. The solubility of $CO_2$ in the PP melts was compared with semiempirical data (determined by empirically measuring gas uptake and theoretically predicting swelling) and theoretical values calculated from the Simha−Somcynsky (SS) and Sanchez−Lacombe (SL) equations of state (EOSs). The Simha−Somcynsky equation of state (SS-EOS) was observed to have a better prediction capacity of the swelling effect and to thus provide better solubility predictions for both semiempirical and theoretical cases than the Sanchez−Lacombe equation of state (SL-EOS).

## Introduction

In a polymer + gas system, solubility is the maximum amount of gas that can be dissolved in the polymer at a specific temperature and pressure without phase separation. Solubility data help to determine processing conditions that are required for applications such as polymer modification, viscosity measurement, blending, and microcellular foaming, where a single-phase solution is mandatory to avoid phase separation.[1,2] In microcellular foaming, cell nucleation is accomplished by a rapid pressure drop that drastically reduces the solubility of the gas in the polymer. This pressure drop governs the final cell morphology and the foam's properties.[3] Consequently, solubility data over a wide range of pressures and temperatures play an important role in processing microcellular foams.[4] Each of the following physical properties of a polymer melt is important in processing and is affected by the amount of dissolved gases contained in the melt: the swollen volume, isothermal compressibility, thermal expansion coefficient,[5] viscosity,[6−8] and surface tension.[9,10] Since the 1950s, much effort has gone into the investigation of gas solubility in polymer melts. Research methods have included experimental measurements and theoretical thermodynamic calculations. Volumetric and gravimetric methods have been widely used to measure the solubility of different blowing agents (BAs) in polymers; however, neither method could solely determine solubility because of the polymer + gas mixture's swelling phenomena, especially at high temperatures and pressures. To accurately measure solubility, the swollen volume or density of the polymer + gas solution must be determined. Swelling due to gas dissolution in the polymer can be obtained either by an EOS prediction or by measurement.[11]

Sato et al. have contributed greatly to the measurement of the solubility of various blowing agents, including supercritical fluids, in a number of foamable resins, and the foaming industry has effectively applied their data.[12−19] Sato et al. concentrated on measuring the solubilities and diffusivities of $CO_2$, $N_2$, hydrofluorocarbons (HFC-I34a, HFC-152a), hydrochlorofluorocarbon (HCFC-142b), *n*-butane, and isobutane in polystyrene (PS), polypropylene (PP), high-density polyethylene (HDPE), polyvinyl acetate (PVAc), biodegradable polymer, polyphenylene oxide (PPO), and PPO + PS blends at various melt temperatures and pressures by using the pressure-decay method or the gravimetric method with a magnetic suspension balance (MSB). However, to estimate the swollen volume due to the dissolved gas, they had to rely on the Sanchez−Lacombe equation of state (SL-EOS), which is used to determine solubility with the pressure-decay or gravimetric methods. Ohshima et al. also used an MSB to determine the solubility of $CO_2$ in low-density polyethylene (LDPE), HDPE, PP, PS, ethylene + ethylacrylate copolymer (EEA), LDPE + titanium dioxide ($TiO_2$) composite, and polypropylene + clay nanocomposites.[20−23] They also used the SL-EOS to calculate the swollen volume of the polymer + gas solution for various concentrations of gas. Handa et al. also investigated the solubility of blowing agents in polymer and liquids.[24,25] They measured the solubility and diffusivity of $CO_2$ in PS, filled polyvinylchloride (FPVC), unplasticized polyvinylchloride (UPVC), and syndiotactic polystyrene (sPS) by using the in situ gravimetric method (i.e., a Cahn D110 electronic microbalance). However, they did not consider the swollen volume caused by gas dissolution in the polymer. Due to a lack of swelling data, most researchers used

* Corresponding author. E-mail: park@mie.utoronto.ca.
[†] University of Toronto.
[‡] University of Waterloo.

10.1021/je100488v 
Published on Web 10/22/2010

an equation of state, such as the SL-EOS, to predict the swelling that determines solubility. Since the validity of the SL-EOS has not been verified yet for the polymer + gas systems, solubility accuracy would be governed by the accuracy of the swollen volume, especially at elevated pressures.

Li et al. also worked extensively on measuring the solubilities of various blowing agents in polymer melts.[26−30] They measured the solubility of $CO_2$ and $N_2$ in PS, PP, HDPE, and polylactic acid (PLA) by using the MSB. They also could not accurately determine blowing agent solubility due to a lack of polymer melt volume swollen experimental data by gas dissolution. Consequently, they too had to rely on equations of state (EOS), such as the Simha-Somcynsky (SS) or Sanchez−Lacombe (SL) EOS with no verified validity, to estimate the swollen volume. They found that the effect of swelling on solubility was more conspicuous at a higher pressure. This was due to increased buoyancy with a higher gas density and the higher swollen volume. They also measured the solubility of HFC134a, HFC152a, and HFC134a + HFC152a blends in PS. They proposed a ternary model for the gas blends + polymer system and determined the solubility pressure to maintain a specific amount and composition of the blends in the PS melt.[29] To study phase equilibria and to determine gas solubility, they applied the following three equations of state to a linear-PP + $CO_2$ system: Sanchez−Lacombe (SL), Simha−Somcynsky (SS), and the Perturbed Chain Statistical Associating Fluid Theory (PC-SAFT).[30] It was found that the interaction parameter in the SL strongly depends on temperature, whereas with the SS and the PC-SAFT, interaction parameters are weak temperature functions. In addition, they noted that the swelling ratios determined by using various equations of state differed from each other and that consequently their solubilities also differed. Since the validity of using these equations of state for predicting the swollen volume was not verified for any polymer + gas mixtures, it was not clear which of them accurately predicted swelling and/or solubility. Li et al. indicated that most published solubility data at elevated pressures might not be accurate and that, therefore, there was a need to first measure the swollen volume to find out which EOS can accurately predict the swollen volume.

Recently, Funami et al. developed a new technique to measure the density of the polymer + gas mixture.[31] They modified the existing MSB system and determined the density of the polymer + gas mixture directly by measuring the buoyancy force exerted on a platinum plate that was submerged in the polymer melt. They measured the densities of polyethylene glycol (PEG) + $CO_2$ and the polyethylene (PE) + $CO_2$ solutions above the melting temperature and at (0 to 15) MPa pressure, and the results were promising. However, their modified MSB is only suitable for low viscous polymers with very low molecular weight. Also, while changing the plate position, the dragging force generates unavoidable measurement errors, especially when the viscosity is high. Gendron et al. also tried to measure the solubility of a $CO_2$ + ethanol blend in PS at various pressures and temperatures using an ultrasonic instrument developed in their laboratory for both off-line and on-line measurement during the extrusion process.[32] They measured the degassing pressures (i.e., the pressure at which phase separation occurs) as a function of temperature by using an ultrasonic signal and found parabolic shape curves. By comparing degassing pressures with MSB data from Sato et al., they concluded that at high temperatures the degassing pressures corresponded reasonably to the solubility data related to the $CO_2$ content. However, since this solubility reflects the dynamic nature of the flow, the dynamic solubility (i.e., the gas solubility) in the oriented molecules may be different from the static solubility. Xanthos and his co-workers measured the dynamic solubility of $CO_2$, $N_2$, and Ar in PS and poly(ethylene terephthalate) (PET) using their self-designed in-line optical window system.[33] They found that the solubility of $CO_2$ in PS decreases with increased throughput in the foaming process and that solubility is independent of screw speed. They also found that data points deviated greatly from the published data in the low-pressure range, and they speculated that this might have been caused by inhomogeneities in the temperature and gas concentration. However, since cell nucleation may not occur easily at a low gas concentration (i.e., at a low pressure), the moment the cell nucleation was observed may not have corresponded to the pressure below the solubility pressure.

Many researchers have also tried to predict swelling phenomena either by measuring the sample's change in lengths[34−40] or by in situ visual observation of the interface position between the gas phase and the polymer melt system.[9−11,41−46] However, sample preparation to release internal stresses and to ensure isotropic behavior is somewhat complicated when measuring sample lengths. Moreover, since the sample shape changes above the glass transition temperature, it is not possible to determine length changes above this temperature. Tomasko and co-workers[41] also tried to measure the solubility of poly(methyl methacrylate) (PMMA) at (303 to 333) K by predicting swelling using an in situ visualization system. They also determined solubility by measuring the mass loss of a polymer sample with regular geometry after removing it from the pressure cell and extrapolating it to zero time. However, this method is limited to a temperature below the glass transition temperature, and experimental solubility data at a high temperature and pressure are rare.

To our knowledge, no literature verifies that the equation of state approach determines the solubility of blowing agents in polymers, especially at high temperatures and pressures. A need, therefore, exists to completely experimentally measure swelling and solubility at higher temperatures and pressures and to compare the results with various EOS approaches to predict the best EOS thermodynamic model. In this study, the solubility of carbon dioxide in linear and branched PP was measured at a high temperature of up to 493 K and a high pressure of up to 31 MPa. Finally, experimental data were compared with semiempirical and theoretical solubility data determined by using the SS and the SL equations of state for accuracy.

***Solubility Determination.*** There are three ways to determine the solubility of gas in a polymer: (i) a theoretical approach based on EOS, (ii) a semiempirical approach, and (iii) an experimental approach.

***Theoretical Approach Based on EOS.*** The solubility of gas in a polymer can be theoretically and independently predicted by an EOS. In this research, only the SS and the SL equations of state (EOSs) were considered. Detailed descriptions of these two equations of state are available in previous publications.[26−30] Brief descriptions appear below, and details of these equations are given in the Supporting Information (SI).

The solubility of gas in a polymer melt can be calculated theoretically using the phase equilibrium theory of multicomponent systems (eq 1). It is assumed that the polymer does not dissolve into the gas phase.

$$\mu_1^G = \mu_1^P \tag{1}$$

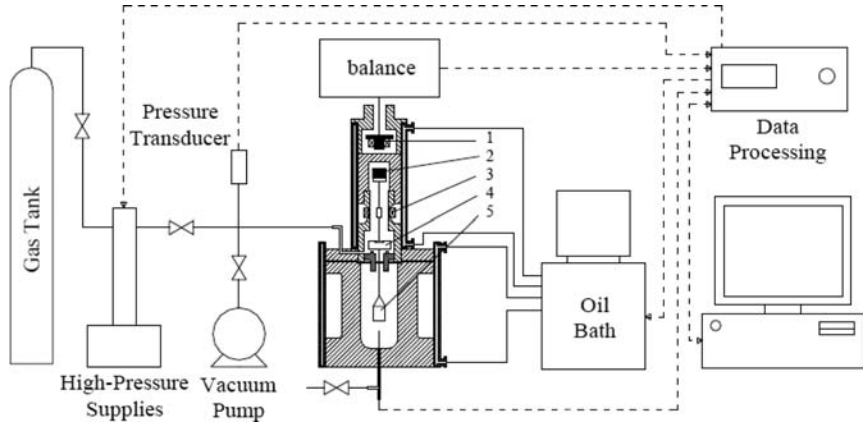


**Figure 1.** Schematic of overall magnetic suspension balance system: 1, electromagnet; 2, permanent magnet; 3, position sensor; 4, coupling device; 5, sample holder.

where $\mu_1^G$ is the chemical potential of gas in the gas phase and $\mu_1^P$ is the chemical potential of gas in the polymer + gas solution phase.

For the SS-EOS, eq 2 was used to calculate the $\mu_1^G$.[47,48]

$$\mu_1^G = \int_v^\infty \left(P - \frac{RT}{V}\right)dV + (PV - RT) + RT\ln\left(\frac{P}{kT}\left(\frac{N_a^2h^2}{2\pi m_1 RT}\right)^{3/2}\right) \quad (2)$$

where $R$ is the universal gas constant; $N_a$ is Avogadro's number; $m_1$ is the molar mass of gas; and $h$ is Planck's constant. Then, eq 3 was used to calculate the $\mu_1^P$ in eq 1.[48]

$$\mu_1^P = G_m + x2\frac{\partial G_m}{\partial x_1} \quad (3)$$

where $G_m$ is the molar Gibbs free energy of the polymer + gas mixture, which was calculated by using eq 4.[48] The details of these equations (1 to 3) can be found in ref 48. Here, subscript 1 refers to gas and 2 refers to polymer.

$$\frac{G_m}{RT} = x_1\ln x_1 + x_2\ln x_2 + \ln(y/s) + s\frac{1-y}{y}\ln(1-y) + (s-1)\ln\frac{e}{z-1} - c[\ln(v^*(1-\eta)^3/Q)] - \frac{3}{2}c_1x_1\ln\frac{2\pi m_1RT}{(N_ah)^2} - \frac{3}{2}c_2x_2\ln\frac{2\pi m_2RT}{(N_ah)^2} + \frac{cyQ^2(1.011Q^2 - 2.409)}{2\tilde{T}} + \frac{c}{ms}\left[(1-\eta)^{-1} + \frac{2yQ^2(1.011Q^2 - 1.2045)}{\tilde{T}}\right] \quad (4)$$

To calculate the $\mu_1^G$ and $\mu_1^P$ in the SL-EOS, eqs 5 and 6 were used, respectively.[49,50]

$$\mu_1^G = r_1^0RT\left[-\frac{\tilde{\rho}_1}{\tilde{T}_1} + \frac{\tilde{P}_1}{\tilde{\rho}_1\tilde{T}_1} + \left(\frac{1}{\tilde{\rho}_1} - 1\right)\ln(1-\tilde{\rho}_1) + \frac{1}{r_1^0}\ln\tilde{\rho}_1\right] \quad (5)$$

$$\mu_1^P = RT\left[\ln\phi_1 + \left(1 - \frac{r_1}{r_2}\right)\phi_2 + r_1^0\tilde{\rho}\frac{P_1^* + P_2^* - 2P_{12}^*}{P_1^*\tilde{T}_1}\phi_2^2\right] + r_1^0RT\left[-\frac{\tilde{\rho}}{\tilde{T}_1} + \frac{\tilde{P}_1}{\tilde{\rho}\tilde{T}_1} + \left(\frac{1}{\tilde{\rho}} - 1\right)\ln(1-\tilde{\rho}) + \frac{1}{r_1^0}\ln\tilde{\rho}\right] \quad (6)$$

The description of these parameters is given in the nomenclature section.

## Experimental Section

***Materials.*** Linear PP (DM 55) and branched PP (Daploy WB130HMS) were procured from Borealis, and carbon dioxide (Coleman grade, 99.99 % purity) was received from BOC Canada. All of these materials were used as received.

***Semi-Empirical Approach.*** Gas solubility can also be determined by empirically measuring gas uptake and theoretically predicting swelling data.

A gravimetric method, the magnetic suspension balance from Rubotherm GmbH, Germany, can be used to measure the sorption of $CO_2$ in polymer melts. A schematic of the magnetic suspension balance system is shown in Figure 1. A detailed description of the experimental apparatus and procedures is available in previous publications,[26−30] and a brief procedure is described below.

Before beginning the sorption experiment, a precisely weighed polymer sample of mass, $m_{sample}$, was placed in the sealed absorption chamber, degassed in the vacuum, and preheated to a designated temperature. The balance readout at vacuum ($P\sim0$) and temperature ($T$) for the polymer sample without any dissolved gas was recorded as $m_{sample}(0,T)$; this value reflected the weight of the sample at vacuum. High-pressure gas was subsequently charged into the chamber, and sorption occurred. When the saturation stage was reached, sorption stopped, and the weight readout from the balance was recorded as $m_{sample}(P,T)$ at pressure ($P$) and temperature ($T$). Hence, weight gain from the dissolved gas in the polymer, $m_{gas}$, was calculated as follows in eq 7

$$m_{gas} = m_{sample}(P,T) - m_{sample}(0,T) + \rho_{gas}(V_B + V_P + V_S) \quad (7)$$

where $\rho_{gas}$ is the density of the gas inside the chamber at temperature $T$ and pressure $P$, which can be measured in situ by the magnetic suspension balance; $V_B$, $V_P$, and $V_S$ are the volumes of the sample holder (i.e., the sample container and

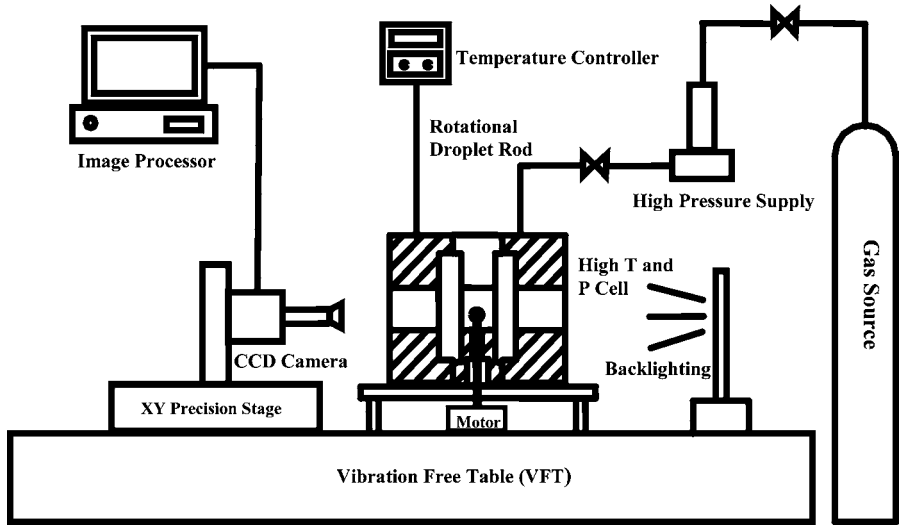


**Figure 2.** Working principle of the in situ visualization system from ref 53.

all measuring load coupling devices), the volume of pure polymer at temperature $T$ and pressure $P$, and the swollen volume of the polymer due to gas dissolution, respectively. $V_B$ is usually determined in advance with a blank experiment. $V_P$ typically can be determined using the Tait equation of state[51] from Gnomix or *PVT* apparatus data for each polymer.

By ignoring the polymer's swollen volume ($V_S$) in eq 7, the measured weight gain of a polymer with mass, $m_{sample}$, at room temperature and pressure, can be transformed to the apparent solubility of eq 8, $X_{apparent}$, which is less than the actual solubility

$$X_{apparent} = \frac{m_{sample}(P,T) - m_{sample}(0,T) + \rho_{gas}(V_B + V_P)}{m_{sample}} \quad (8)$$

The $X_{apparent}$ was calculated using the magnetic suspension balance. As shown in eqs 7 and 8, it is impossible to accurately measure gas solubility in the polymer melt without considering the swollen volume ($V_S$). To accurately determine solubility, correction of the buoyancy effect on the apparent solubility data is essential, especially in a high-pressure condition where gas density (i.e., $\rho_{gas}$) is high and the swollen volume (i.e., $V_S$) is large.

As long as the interaction parameters and all scaling parameters in the EOS are known, the specific volume of the mixture can be calculated by solving either the SS-EOS (eqs 9 and 10)[47,48]

$$\tilde{p}\tilde{V}/\tilde{T} = (1-\eta)^{-1} + \frac{2yQ^2(1.011Q^2 - 1.2045)}{\tilde{T}} \quad (9)$$

$$\left(\frac{s}{3c}\right)\left[\frac{s-1}{s} + \frac{\ln(1-y)}{y}\right] = \frac{\eta - 1/3}{1-\eta} + \frac{y}{6\tilde{T}}Q^2(2.409 - 3.033Q^2) \quad (10)$$

or the SL-EOS (eq 11).[49,50]

$$\tilde{P} = -\tilde{\rho}^2 - \tilde{T}\left[\ln(1-\tilde{\rho}) + \left(1 - \frac{1}{r}\right)\tilde{\rho}\right] \quad (11)$$

In the above relations, $\tilde{P}$, $\tilde{V}$, $\tilde{\rho}$, and $\tilde{T}$ are reduced parameters. They are calculated from the characteristic reducing parameters $P^*$, $T^*$, $V^*$, and $\rho^*$, which are defined as $1/\tilde{\rho} = V/V^*$, $\tilde{T} = T/T^*$, $\tilde{P} = P/P^*$, $\tilde{V} = V/V^*$, and $r = (MP^*)/(RT^*\rho^*)$. Here, $y$ is the fraction of occupied lattice sites; $s$ is the number of segments per chain of molar mass; $c$ is the number of external degrees of freedom per chain; and $Q = 1/y\tilde{V}$ and $\eta = 2^{-1/6}yQ^{1/3}$ are dimensionless quantities.

As specified by the SS-EOS theory, polymer segment sizes should be adjusted so that the molar repulsion volumes of the polymer segments match those of the gas molecules. Therefore, for the polymer + gas system we were studying, the SS and the SL equations of state scaling parameters were obtained for both PP. Our previous paper lists all scaling parameters for each component (in both the SS- and the SL-EOSs),[28] and information can also be found in the SI. The swollen volume was then predicted using the SS- and the SL-EOSs. This was coupled in eq 12 to determine the semiempirical solubility as follows

$$X_{corrected} = X_{apparent} + \frac{\rho_{gas}V_S}{m_{sample}} \quad (12)$$

No matter which EOS was used, both theoretical and corrected solubilities were highly dependent on the interaction parameters ($\delta_e$, $\delta_v$ for the SS, and $k_{12}$ for the SL equations of states). In our research,[26−30] we proposed that the EOS is capable of accurately computing the theoretical solubility ($X_{theory}$) and the swollen volume ($V_S$) of the polymer + gas mixture simultaneously. The optimal interaction parameters for each EOS are determined by searching for the minimum deviation between $X_{corrected}$ and $X_{theory}$. We presented a more detailed procedure on extracting optimal interaction parameters in our previous publications.[26−30]

***Experimental Approach.*** Gas solubility can also be fully determined by empirical measurements. Instead of predicting the $V_S$ in eq 12 using an EOS, it can be directly measured using a high-pressure, high-temperature cell.[11,52,53]

The schematic of the experimental setup of the *PVT* apparatus is illustrated in Figure 2. Details of the apparatus and procedure can be found in our previous work.[11,52,53] It is assumed that the polymer pendent or sessile drop is axisymmetric to start with, which means the droplet profile is symmetrical with its vertical centerline. At the beginning of each experiment, the

camera parameters, such as the working distance relative to the drop sample and the image contrast through the optical lens, are adjusted for maximum zoom. At the same time, care is taken to ensure the best image quality at the boundary. A calibration is then made to determine the pixel size in *x* and *y* orientation, with regard to the XY stage movement. Since the unit step length of the stage is known, calibration determines the size of the pixel's metric length based on the stage's movement. This part of the procedure is crucial because it provides the conversion factor between the image pixel size and the real drop's metric dimension during image reconstruction. It also helps to correct any potential optical distortion.

The number of images that will cover the whole pendant/sessile drop is calculated based on the magnification of the optical system and the CCD camera's resolution. For a given number, the stepwise movements of the XY stage in both *x* and *y* directions are determined. Those *x* and *y* increments are programmed and stored into the motion controller to guide the step motor to move the XY stage and camera with precision. The images are captured when the camera pauses briefly in between each new *x* and *y* movement. The series of images is then combined and reconstructed to form a complete drop image based on the movements using an image processing tool.

When the image reconstruction is complete, the precise edge detection algorithm is used to detect the drop boundary and to generate the edge pixel coordinates. The Canny edge detector,[54] which is based on the first derivative and defines the detection and localization criteria of a class of edges, is the most successful subpixel edge detector. It is used to identify boundary profile coordinates. To improve the accuracy of drop profile coordinates, repeated points (i.e., a pixel with the same gray levels at one location) are averaged into distinctive data points ($x_i$, $x_j$) using a smoothing technique. The drop profile could be represented using an $f(x)$ notation after a spline fits through all the points.

The composite Simpson's 1/3 method, which has superior and finer segments than the Trapezoidal rule, was selected from other numerical integration methods.[55] The trapezoidal rule for integration finds the area under the line connecting the end points of a panel, whereas Simpson's rule finds the area under the parabola which passes through three points on a curve. In other words, the rule approximates the curve by a series of parabolic arcs, and the area under the parabolas is approximately the area under the curve. However, in most of the cases, the function which needs to be integrated may not be smooth over the entire interval. This may be caused from the oscillatory function or the lack of derivatives at certain points. In such cases, Simpson's rule may give very poor results. One of the best ways to resolve this problem is by breaking up the interval into a number of small subintervals. Simpson's rule is then applied to each subinterval, with the results being summed to produce an approximation for the integral over the entire interval. This approach is termed as composite Simpson's rule. Therefore, composite Simpson's 1/3 rule was applied for integration to compute the final volume of the polymer + gas solution drop, and it takes the following form in eqs 13 and 14

$$I = \int_a^b f(x)\mathrm{d}x = \frac{1}{3}h[f(x_0) + 4\sum_{i=1,3,5}^{n-1} f(x_i) + 2\sum_{j=2,4,6}^{n-2} f(x_j) + f(x_n)] \quad (13)$$

where $h$ is the "step length" between the interval [$a$, $b$], which is split up in subintervals $n$ and given by

$$h = \frac{(b-a)}{n} = \frac{(x_n - x_1)}{n} \quad (14)$$

For volume integration, Simpson's 1/3 rule is expressed and approximated in eqs 15 to 18 in drop profile points as follows

$$V_{\text{total}} = \int_a^b \pi \cdot f(x)^2 \mathrm{d}x \cong \frac{1}{3}\cdot\pi\cdot h\cdot \sum_{i,j}^{N} (R_{i,j}^2 + R_{i,j}\cdot r_{i,j+1} + r_{i,j+1}^2) \quad (15)$$

where

$$R_{i,j} = (x_{2N+1-i,j} - x_{i,j})/2 \quad (16)$$

$$r_{i,j+1} = (x_{2N+1-i,j+1} - x_{i,j+1})/2 \quad (17)$$

$$h = (x_j - x_1)/N \quad (18)$$

where $V_{\text{total}}$ is the total volume of the drop; $R_{i,j}$ is the radius of drop at the $j$th layer; $r_{i,j+1}$ is radius of the drop at the $j+1$th layer; and $f(x)$ represents the drop profile function. Also $i = 1, 2, ..., 2N$ (in the $x$-direction) and $j = 1, 2, ..., N$ (in $y$-direction), and $2N$ is the total number of pixel points.

The volume swelling ratio, $S_w$ (eq 19), in this study was defined by comparing the final equilibrium volume with the initial volume, which was calculated using the Tait equation as follows

$$S_w = \frac{V(T,P,t_{eq})}{V(T,P,t_{ini})} = \frac{V(T,P,t_{eq})}{m_{\text{sample}}v(T,P)} \quad (19)$$

where $V(T,P,t_{eq})$ is the measured equilibrium polymer + gas solution volume at temperature $T$, pressure $P$, and equilibrium time $t_{eq}$; $V(T,P,t_{ini})$ is the volume of the neat PP sample calculated at temperature $T$ and pressure $P$ using the Tait equation which was derived from Gnomix apparatus data. Once $V_S$ was determined, the experimental solubility of $CO_2$ was determined by using the $V_S$ value in eq 12 where $X_{\text{apparent}}$ was determined by using the magnetic suspension balance.

***Experimental Verification.*** The proposed reconstruction methodology was already verified in our previous publication by measuring the volume of a precision stainless steel sphere with a known volume and by comparing the specific volume data measured from this methodology and from the Gnomix method.[11] Details are given in ref 11 and the SI.

***Uncertainty Analysis.*** A magnetic suspension balance from Rubotherm GmbH, Germany, was used to measure the solubility. The resolution of the balance is 10 $\mu$g with a relative error of less than 0.002 % of the measured value. The reproducibility (standard deviations) of the machine is ± 20 $\mu$g. Each experiment was conducted at least three times to obtain repeatability of the proposed data. Since the solubility is not a directly measured quantity, various factors contribute toward the precision of the solubility results. Uncertainty in the pressure measurement is ± 0.5 % of reading, and temperature was ± 0.1 K. There was some uncertainty of the solubility resulting from each experiment, and the maximum uncertainty was found to be less than ± 4 % with a 95 % level of confidence. This statistical analysis is suitable for a small number of observations.[56]

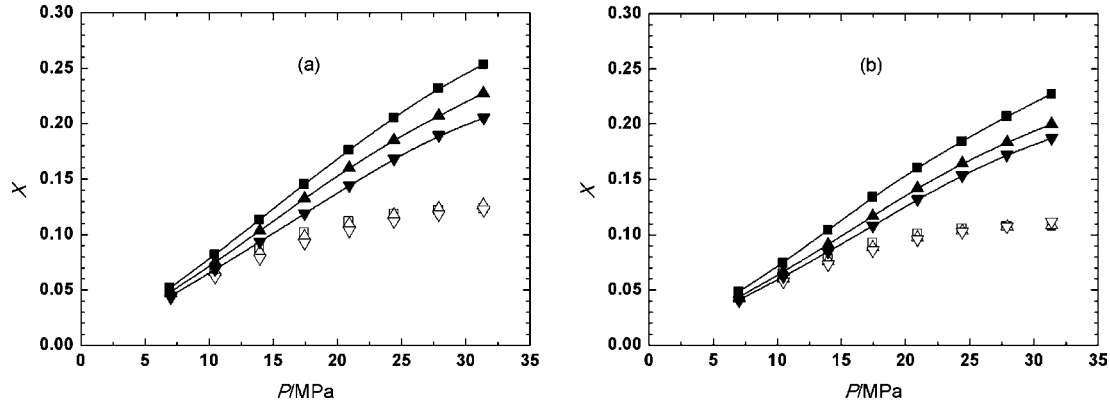


**Figure 3.** Experimental solubility, $X$ (g of gas/g of polymer) of $CO_2$ in PP: (a) linear PP; (b) branched PP; ■, 453 K, corrected; □, 453 K, apparent; ▲, 473 K, corrected; △, 473 K, apparent; ▼, 493 K, corrected; ▽, 493 K, apparent.

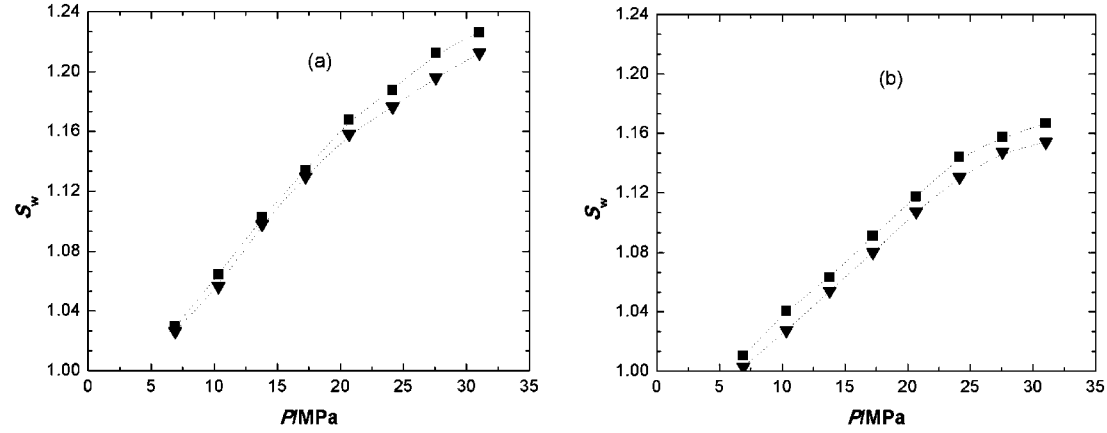


**Figure 4.** Comparison of swelling ratio, $S_w$: ■, linear PP; ▼, branched PP; (a) 453 K; (b) 493 K, ref 53.

## Results and Discussion

***Solubility of $CO_2$ in Linear and Branched PP.*** As discussed in the previous section, the solubility of $CO_2$ in both linear and branched PP was completely experimentally measured at (453 to 493) K temperature and at a pressure of up to 31 MPa. The maximum pressure and temperature that can be attained in the magnetic suspension balance chamber is 34.5 MPa and 523 K, respectively. All the experimental data are given in Tables 1 to 6 in the SI.

Once the swelling ratio was measured by the *PVT* apparatus,[53] the empirical solubility was determined by using the magnetic suspension balance to measure the apparent solubility and by putting the value of the swollen volume into eq 19. Figure 3 shows the solubility of $CO_2$ in linear and branched PP, respectively. It was observed that solubility increases as pressure increases but that it decreases as temperature increases for both polymers. Other researchers have observed a similar trend.[12−23,26−30] When a polymer melt is subjected to a high-pressure gas, two competing mechanisms affect the specific volume of the polymer + gas mixture: (i) the hydrostatic pressure effect and (ii) swelling due to gas absorption.[11,53] Hydrostatic pressure acts to decrease the specific volume, as well as the free volume, whereas swelling helps to increase both of them. Usually swelling is more dominant when gas goes into the polymer. Dissolved $CO_2$ causes a plasticization effect that reduces viscosity. This increases chain mobility by increasing the free volume and reducing surface tension, both of which are critical microcellular foaming parameters. It was also noted that solubility is concave to the pressure axis. In other words, after a certain pressure, solubility did not increase linearly with increasing pressure. Rather, the solubility of $CO_2$ in both PP melts shows a leveling off trend above 31 MPa. Wissingner et al.[34] and Rajendrain et al.[44] also observed a similar trend. Rajendrain et al. used the magnetic suspension balance to measure the solubility of $CO_2$ in PMMA at temperatures ranging from (323 to 353) K and at pressures of up to 25 MPa. They also measured the swollen volume by using in situ visualization. They found both swelling and solubility curves began to level off above 15 MPa. Knez and co-workers applied the SL and the PC-SAFT EOS to predict the solubility of supercritical $CO_2$ in poly(L-lactide) and poly(D,L-lactide) + glycolide at three different temperatures between (308 and 323) K and up to a 30 MPa pressure.[57] They found that the solubility curve is concave to the pressure axis and starts to level off at high pressures (above 15 MPa). They also claimed that both the SL and PC-SAFT were reliable models to describe the phase equilibrium of PLLA + $CO_2$ and PLGA + $CO_2$ systems under the proposed working conditions.

It was further found that linear PP absorbs more $CO_2$ than branched PP for a particular temperature and pressure, especially at a higher pressure. This is due to the swelling effect discussed in an earlier paper.[53] It is believed that the branched molecular chain structure causes greater entanglement, which can generate a higher resistance to volume expansion. Therefore, a branched chain structure generates less accommodation for small gas molecules dissolving into the polymer melt and exhibits a less swollen volume than a linear chain structure (Figure 4). According to Hiemenz,[58] branched polymer chains result from the presence of monomer with a functionality of greater than two. This branching might produce a three-dimensional network of polymer. The solubility and mechanical behavior of branched polymers largely depend on whether the extent of polymerization is above or below the threshold (gel point) for the formation of

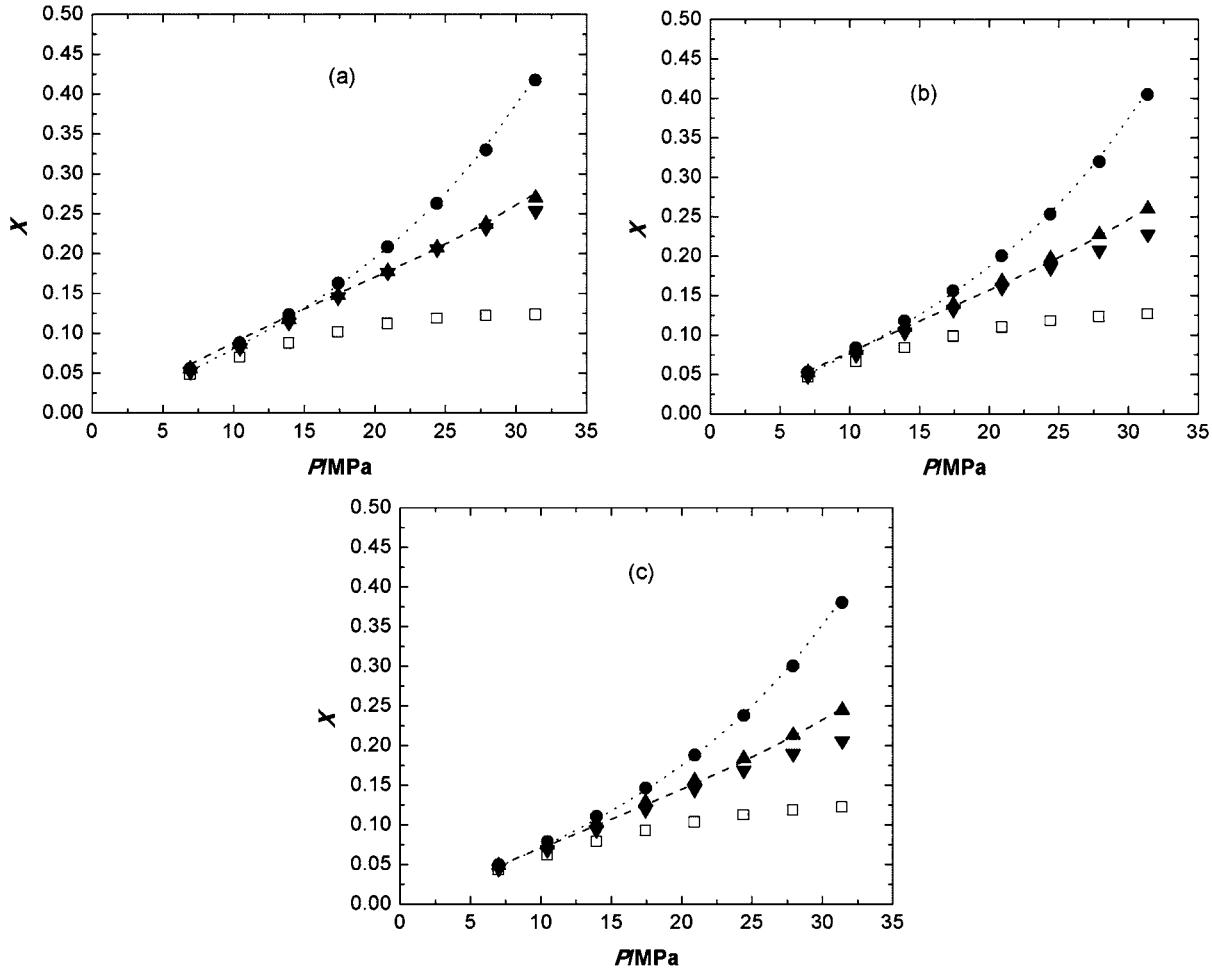


**Figure 5.** Comparison of experimental, semiempirical, and EOS-based solubility, $X$ (g of gas/g of polymer), of $CO_2$ in linear PP: ●, SL-EOS corrected; ⋯, SL-EOS theoretical; ▲, SS-EOS corrected; --, SS-EOS theoretical; ▼, experimental; □, apparent; (a) 453 K; (b) 473 K; (c) 493 K.

such a network. Hiemenz has also shown several reaction possibilities in the presence of multifunctional reactants. Though branched PP helps to increase the melt strength of the PP blend, it is obvious that the addition of branched PP to linear PP will decrease the overall solubility. However, interesting is the question of how much short-chain or long-chain branching affects solubility, which is beyond the research scope of this paper to answer.

***Comparison of Solubility—Theoretical, Semiempirical, and Experimental Values.*** As is well-known, solubility data that were determined completely experimentally would have much greater accuracy and reliability. After we determined solubility experimentally, we compared the results with our previous data, which had been calculated using the SS- and the SL-EOSs.[28] All the characteristic parameters for the polymers and gas are given in Table 7 in the SI. The solubility of $CO_2$ determined from the SS- and the SL-EOSs for both linear and branched PP is shown in Figures 5 and 6, respectively. It was observed that for both types of PP the solubility predicted by the SS and the SL was quite close to the experimental value at a low temperature and pressure (i.e., less than 13.8 MPa), but the SS showed a better agreement at higher temperatures and pressures compared with the SL. This is due to the swollen volumes determined by the SL- and SS-EOSs, which are shown in Figures 7 and 8. Since the swollen volume predicted by the SL is higher than that predicted by the SS, the semiempirical and theoretical solubilities determined by the SL are also higher than the SS-EOS. These results indicate that the SS is able to predict solubility more accurately than the SL-EOS. The SS and SL, along with four other theoretical equations of state, have been comprehensively tested for *PVT* data in 56 polymers by Rodgers.[59] The SS-EOS shows excellent capabilities for describing polymer melt *PVT* data over a wide range of temperatures and pressures. Moreover, the application of the SS-EOS in the multicomponent fluid system used to predict the mixture's *PVT* behavior has been previously studied.[47,48] The SS-EOS might be a good candidate to predict the *PVT* behavior of a polymer + gas mixture.

The SL has been extensively used to predict the solubility of blowing agents in polymer melts because of its simplicity. Recently, however, several researchers have tried to modify the SL to better correlate it with experimental data.[60,61] To this end, Machida et al. tried to modify the interaction energy parameter ($\varepsilon^*$) of the SL-EOS.[60] Since hydrogen bonding and ionic interaction depend on temperature, they modified the interaction energy term as a function of temperature in the form of the Langmuir equation to manage the temperature effect. Then they compared the modified SL with the original one by computing the volumetric data for the group of nonpolar fluids, polar fluids, and ionic liquids and claimed that the modified SL provides better *PVT* representation and could be used for mixtures. Krenz et al. also tried to modify the original SL-EOS adopting Neau's modified SL and included a Peneloux-type volume translation.[61] They proposed that the modified SL equation can perform vapor−liquid equilibrium (VLE), liquid−liquid equilibrium (LLE), and vapor−liquid−liquid equilibrium (VLLE) calcula-

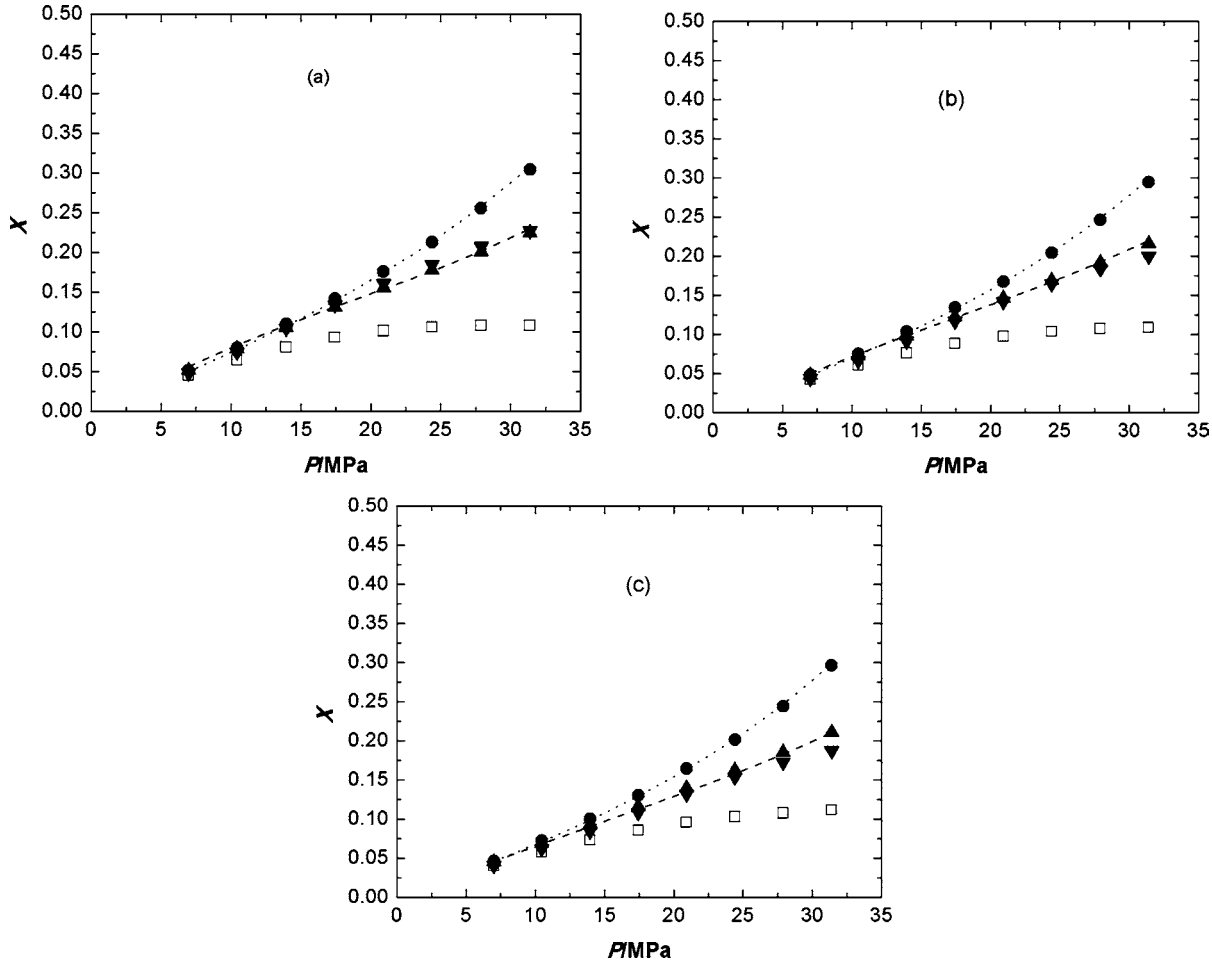


**Figure 6.** Comparison of experimental, semiempirical, and EOS-based solubility, $X$ (g of gas/g of polymer) of $CO_2$ in branched PP: ●, SL-EOS corrected; ···, SL-EOS theoretical; ▲, SS-EOS corrected; --, SS-EOS theoretical; ▼, experimental; □, apparent; (a) 453 K; (b) 473 K; (c) 493 K.

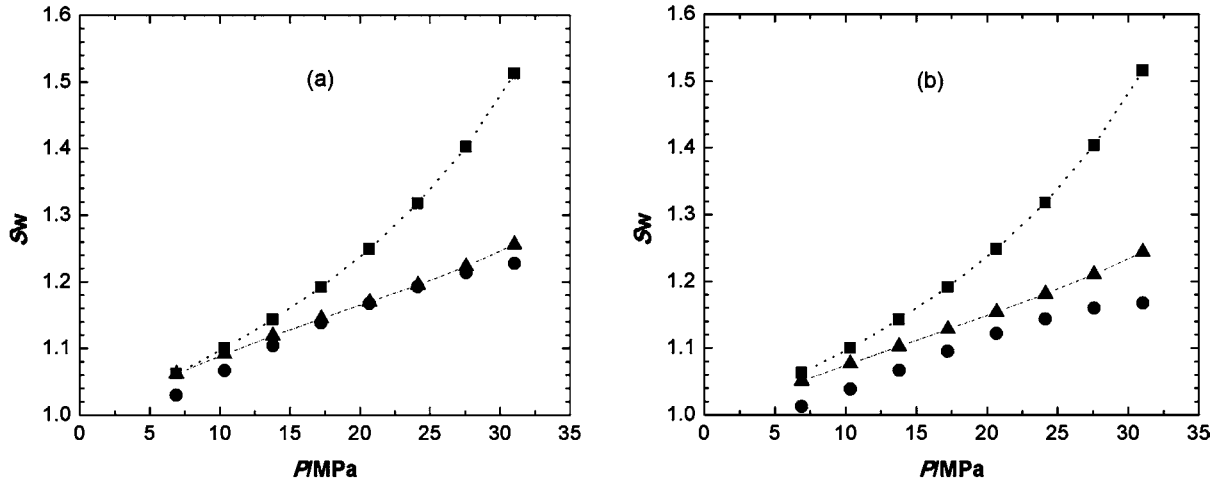


**Figure 7.** Comparison of experimental and EOS swelling ratio, $S_w$, for linear PP: ■, SL-EOS; ▲, SS-EOS; ●, *PVT* experiment; (a) 453 K; (b) 493 K, ref 53.

tions for polyethylene + ethylene + hexane mixtures across a wide range of temperatures, pressures, and compositions.

On the other hand, the swollen volumes predicted by the SS-EOS for both PPs are still much higher than the experimental data at a higher temperature and at any pressure (see Figures 7b and 8b). This indicates that the SS should be modified for predicting the *PVT* behavior of the polymer + gas mixture more accurately, especially at high temperatures. Recently, a few researchers tried to modify the SS-EOS to better correlate it with the experimental data.[62−65] On the basis of the statistical theory for the thermal defects of an imperfect crystal, Zhong et al. proposed an exponential relation between occupied-site fraction ($y$) and reduced temperature ($\tilde{T}$) and developed a simplified SS-EOS version.[62,63] They then applied the modified SS to determine the *PVT* behavior of 11 polymers and found it very promising. Wang et al. realized that although the SS can predict the *PVT* behavior of polymer much better than other EOSs, it does not predict as well for gases at low pressures.[64]

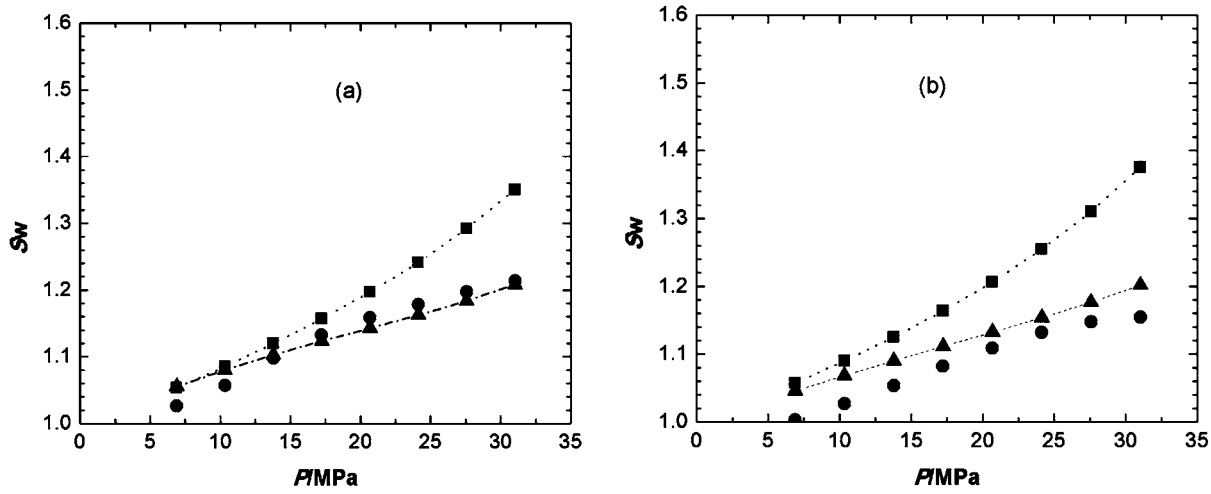


**Figure 8.** Comparison of experimental and EOS swelling ratio, $S_w$, for branched PP: ■, SL-EOS; ▲, SS-EOS; ●, *PVT* experiment; (a) 453 K; (b) 493 K, ref 53.

They proposed to modify the free volume contribution of the SS by incorporating the perturbed hard-chain theory of Beret and Prausnitz with two universal constants to the free volume term. They also determined the characteristic parameters for the modified SS-EOS for 44 low molecular weight substances and 64 polymers. They then calculated the absolute average deviations (AADs) for critical temperature, critical pressure, and vapor pressures, which they found to be very reasonable, while AAD for critical density and saturated liquid density at the normal boiling point were a bit larger. We also found that though swelling predicted by the SS-EOS at high temperature (Figures 7b and 8b) is way off from the empirical data, only the swelling at high pressure has a significant effect on solubility determination (Figures 5 and 6). This suggests that modification of the SS-EOS is necessary for better prediction of swelling and solubility especially for high temperatures and pressures.

Since all of the above modifications for both the SS- and the SL-EOSs are based on experimental data, the validity of these modifications strongly depends on the empirical value. To predict the *PVT* behavior of the polymer + gas solution, further modification of the SS-EOS is required. To accomplish this modification, more accurate solubility data with a wide range of temperatures and pressures are essential.

## Conclusion

Whether a gravimetric or volumetric method is used to measure the solubility of blowing agents (BAs) in polymer, an EOS has been used to compensate for the buoyancy effect of swelling that occurs due to gas dissolution. As a result of this limitation, the obtained solubility data are inadequate, especially at a high pressure where swelling is dominant. A magnetic suspension balance combined with a *PVT* apparatus was successfully applied to study the swelling behavior of linear and branched PP + $CO_2$ solutions and to determine the solubility of $CO_2$ in those polymers at high temperatures and pressures. It was noted that branched PP swells less than linear PP due to the entanglement effect of branched PP. Thus, branched PP can only accommodate a smaller amount of gas, resulting in a decreasing solubility trend. For both linear and branched PP, the hydrostatic effect of pressure is clearly shown at a high pressure (i.e., above 21 MPa), and the volume swelling ratio eventually approaches a plateau region.

Since the SL- and the SS-EOSs are widely used to determine the swollen volume of a polymer + gas solution or to determine the solubility of blowing agents in polymers that have different values, the EOSs should be verified. From these results, some inferences can be made regarding EOS accuracy. Since various equations of state are used to determine the solubility of blowing agents, the SS-EOS might be one of the best candidates to accurately predict the solubility of gas in polymer. In the future, the SS-EOS will be modified to better correlate with the empirical data, especially at high temperatures and pressures.

### Nomenclature

| | |
|---|---|
| $c_i$ | chain (molecule) flexibility; 3c is total external degrees of freedom attributed to a chain (molecule) |
| $G_m$ | molar Gibbs free energy for polymer/gas mixture [J·mol$^{-1}$] |
| $h$ | Planck's constant 6.6260755·10$^{-34}$ [J·s$^{-1}$] |
| $k$ | Boltzmann's constant 1.380658·10$^{-23}$ [J·K$^{-1}$] |
| $m_i$ | molar mass of segment (mer) of "$i$" component [g·mol$^{-1}$] |
| $M$ | molecular weight of per molecule [g·mol$^{-1}$], $M = m_i s_i$ |
| $N_a$ | Avogadro's number, 6.0221367·10$^{23}$ |
| $P$ | pressure [Pa] |
| $P_i$* | characteristic pressure of component "$i$" [Pa], $P_i^* = (qz\varepsilon_i^*)/(sv_i^*)$ |
| $\tilde{P}$ | reduced pressure $P/P^*$ |
| PC-SAFT | Perturbed Chain Statistical Associating Fluid Theory |
| $q_i z$ | the number of nearest neighbor sites per chain-like molecule (s-mer), $s_i(z-2)+2$ |
| $Q$ | $(y\tilde{V})^{-1}$, dimensionless identity |
| $\tilde{\rho}$ | reduced density $1/\tilde{V}$ |
| $r$ | number of mer per molecule, $r = (MP^*)/(RT^*\rho^*)$ |
| $R$ | gas constant, 8.3143 [J·(mol·K)$^{-1}$] |
| $s_i$ | number of mers per molecule of component "$i$" |
| SL | Sanchez−Lacombe |
| SS | Simha−Somcynsky |
| $S_w$ | volume swelling ratio |
| $T$ | temperature [K] |
| $T_i$* | characteristic temperature of component "$i$" [K], $T_i^* = (qz\varepsilon_i^*)/(cK)$ |
| $\tilde{T}$ | reduced temperature $T/T^*$ |
| $v_i$* | characteristic volume per mer of component "$i$" [m$^3$·mer$^{-1}$] |
| $V_i$* | characteristic volume of component "$i$" (m$^3$·mol$^{-1}$) |
| $\tilde{V}$ | reduced volume $V/V^*$ |
| $x_i$ | mole fraction of "$i$" component in mixture system |
| $X$ | solubility (g of gas/g of polymer) |

| | |
|---|---|
| $y$ | occupied lattice site fraction |
| $z$ | 12, the lattice coordination number |
| $\varepsilon_i$* | characteristic energy per mer of component "*i*" ($J \cdot mer^{-1}$) |
| $\eta$ | $2^{-1/6} y Q^{1/3}$ dimensionless number |
| $\phi_1$ | volume fraction of gas in mixture system |
| $\phi_2$ | volume fraction of polymer in mixture system |
| $\mu_1^G$ | chemical potential of gas in vapor phase [$J \cdot mol^{-1}$] |
| $\mu_1^P$ | chemical potential of gas in the polymer melt [$J \cdot mol^{-1}$] |
| $\rho$* | characteristic density of bulk material [$g \cdot cm^{-3}$] |

*Subscripts*

| | |
|---|---|
| 1 | gas |
| 2 | polymer |
| *i* | component number or component in *x*-direction |
| *j* | component number in *y*-direction |

*Superscripts*

| | |
|---|---|
| G | gas or vapor |
| P | polymer |

**Supporting Information Available:**

All the experimental data with standard deviations are shown in Tables 1−6. The characteristic parameters used for both SS-EOS and SL-EOS are given in Table 7. The equations for Gibbs free energy for SS-EOS are also shown. This material is available free of charge via the Internet at http://pubs.acs.org.

## Literature Cited


(1) Tomasko, D. L.; Li, H.; Liu, D.; Han, X.; Wingert, M. J.; Lee, L. J.; Koelling, K. W. A review of $CO_2$ applications in the processing of polymers. *Ind. Eng. Chem. Res.* **2003**, *42*, 6431–6456.

(2) Elkovitch, M. D.; Tomasko, D. L.; Lee, L. J. Supercritical carbon dioxideassisted blending of polystyrene and poly(methyl methyacrylate). *Polym. Eng. Sci.* **1999**, *39*, 2075–2084.

(3) Xu, X.; Park, C. B.; Xu, D.; Pop-Iliev, R. Effects of die geometry on cell nucleation of PSfoams blown with $CO_2$. *Polym. Eng. Sci.* **2003**, *43*, 1378–1390.

(4) Li, G. Thermodynamic investigation of the solubility of physical blowing agents in polymer melts. Ph.D. Theses, MIENG University of Toronto, 2007.

(5) Garg, A.; Gulari, E.; Manke, C. W. Thermodynamics of polymer melts swollen with supercritical gases. *Macromolecules* **1994**, *27*, 5643–5653.

(6) Park, H. E.; Dealy, J. M. Effects of pressure and supercritical fluids on the viscosity of polyethylene. *Macromolecules* **2006**, *39*, 5438–5452.

(7) Gendron, R.; Champagne, M. F. Effect of physical foaming agents on the viscosity of various polyolefin resins. *J. Cell. Plastics* **2004**, *40*, 131–143.

(8) Lee, M.; Tzoganakis, C.; Park, C. B. Effects of supercritical $CO_2$ on the viscosity and morphology of polymer blends. *Adv. Polym. Technol.* **2000**, *19*, 300–311.

(9) Li, H.; Lee, L. J.; Tomasko, D. L. Effect of carbon dioxide on the interfacial tension of polymer melts. *Ind. Eng. Chem. Res.* **2004**, *43*, 509–514.

(10) Xue, A.; Tzoganakis, C.; Chen, P. Measurement of interfacial tension in PS/LDPE melts saturated with supercritical $CO_2$. *Polym. Eng. Sci.* **2004**, *44*, 18–27.

(11) Li, Y. G.; Park, C. B.; Li, H. B.; Wang, W. Measurement of the *PVT* property of PP/$CO_2$ solution. J. *Fluid Phase Equilib.* **2008**, *270*, 15–22.

(12) Sato, Y.; Yurugi, M.; Fujiwara, K.; Takishima, S.; Masuoka, H. Solubilities of carbon dioxide and nitrogen in polystyrene under high temperature and pressure. *Fluid Phase Equilib.* **1996**, *125*, 129–138.

(13) Sato, Y.; Yurugi, M.; Fujiwara, K.; Takikawa, T.; Sumarno; Takishima, S.; Masuoka, H. Solubilities and diffusion coefficients of carbon dioxide and nitrogen in polypropylene, high-density polyethylene, and polystyrene under high pressures and temperatures. *Fluid Phase Equilib.* **1999**, *162*, 261–276.

(14) Sato, Y.; Takikawa, T.; Sorakubo, A.; Takishima, S.; Masuoka, H.; Imaizumi, M. Solubility and diffusion coefficient of carbon dioxide in biodegradable polymers. *Ind. Eng. Chem. Res.* **2000**, *39*, 4813–4819.

(15) Sato, Y.; Iketani, T.; Takishima, S.; Masuoka, H. Pol. Solubility of hydrofluorocarbon (HFC-I34a, HFC-152a) and hydrochlorofluorocarbon (HCFC-142b) blowing agents in polystyrene. *Polym. Eng. Sci.* **2000**, *6*, 1369–1375.

(16) Sato, Y.; Takikawa, T.; Takishima, S.; Masuoka, H. Solubilities and diffusion coefficients of carbon dioxide in poly(vinyl acetate) and polystyrene. *J. Supercrit. Fluids* **2001**, *19*, 187–198.

(17) Sato, Y.; Takikawa, T.; Yamane, M.; Takishima, S.; Masuoka, H. Solubility of carbon dioxide in PPO and PPO/PS blends. *Fluid Phase Equilib.* **2002**, *847*, 194–197.

(18) Sato, Y.; Wangi, Y.; Takishima, S.; Masuoka, H.; Watanabe, T.; Fukasawa, Y. Solubility of butane and isobutane in molten polypropylene and polystyrene. *Polym. Eng. Sci.* **2004**, *44*, 2083–2089.

(19) Wang, M.; Sato, Y.; Iketani, T.; Takishima, S.; Masuoka, H.; Watanabe, T.; Fukasawa, Y. Solubility of HFC-134a, HCFC-142b, butane, and isobutane in low-density polyethylene at temperatures from 383.15 to 473.15K and at pressures up to 3.4 MPa. *Fluid Phase Equilib.* **2005**, *232*, 1–8.

(20) Areerat, S.; Naguta, T.; Ohshima, M. A measurement and prediction of LDPE/$CO_2$ solution viscosity. *Polym. Eng. Sci.* **2002**, *42*, 2234–2245.

(21) Areerat, S.; Funami, E.; Hayata, Y.; Nakagawa, D.; Ohshima, M. Measurement and prediction of diffusion coefficients of supercritical $CO_2$ in molten polymers. *Polym. Eng. Sci.* **2004**, *44*, 1915–1924.

(22) Areerat, S.; Hayata, Y.; Katsumoto, R.; Kegasawa, T.; Egami, H.; Ohshima, M. Solubility of carbon dioxide in polyethylene/titanium dioxide composite under high pressure and temperature. *J. Appl. Polym. Sci.* **2002**, *86*, 282–288.

(23) Taki, K.; Yanagimoto, T.; Funami, E.; Okamoto, M.; Ohshim, M. Visual observation of CO2 foaming of polypropylene-clay nanocomposites. *Polym. Eng. Sci.* **2004**, *44*, 1004–1011.

(24) Wong, B.; Zhang, Z.; Handa, Y. P. High-Precision gravimetric technique for determining the solubility and diffusivity of gases in polymers. *J. Polym. Sci., Part B: Polym. Phys.* **1998**, *36*, 2025–2032.

(25) Varma-Nair, M.; Handa, P. Y.; Mehtab, A. K.; Agarwal, M. Effect of compressed $CO_2$ on crystallization and melting behavior of isotactic polypropylene. *Thermochim. Acta* **2003**, *396*, 57–65.

(26) Li, G.; Lia, H.; Turng, L. S.; Gong, S.; Zhang, C. Measurement of gas solubility and diffusivity in polylactide. *Fluid Phase Equilib.* **2006**, *246*, 158–166.

(27) Li, G.; Gunkel, F.; Wang, J.; Park, C. B.; Altstädt, V. Solubility measurements of $N_2$ and $CO_2$ in polypropylene and ethene/octene copolymer. *J. Appl. Polym. Sci.* **2007**, *103*, 2945–2953.

(28) Li, G.; Wang, J.; Park, C. B.; Simha, R. Measurement of gas solubility in linear/branched PP melts. *J. Polym. Sci., Part B: Polym. Phys.* **2007**, *45*, 2497–2508.

(29) Li, G.; Leung, S. N.; Hasan, M.; Wang, J.; Park, C. B.; Simha, R. A. thermodynamic model for ternary mixture systems—Gas blends in a polymer melt. *Fluid Phase Equilib.* **2008**, *266*, 129–142.

(30) Li, G.; Wang, J.; Park, C. B. Investigating the solubility of $CO_2$ in polypropylene using various EOS models. *Cell. Polym.* **2006**, *25*, 237–248.

(31) Funami, E.; Taki, K.; Ohshima, M. Density Measurement of polymer/$CO_2$ single-phase solution at high temperature and pressure using a gravimetric method. *J. Appl. Polym. Sci.* **2007**, *105*, 3060–3068.

(32) Gendron, R.; Champagne, M.; Delaviz, Y.; Polasky, M. E. Polystyrene with a mixture of $CO_2$ and ethanol. *J. Cell. Plast.* **2006**, *42*, 127–138.

(33) Zhang, Q.; Xanthos, M.; DEY, S. K. Parameters affecting the in-line measurement of gas solubility in thermoplastic melts during foam extrusion. *J. Cell. Plast.* **2001**, *37*, 284–292.

(34) Wissinger, R. G.; Paulaitis, M. E. Swelling and sorption in polymer-$CO_2$ mixtures at elevated pressures. *J. Polym. Sci., Part B: Polym. Phys.* **1987**, *25*, 2497–2510.

(35) Zhang, Y.; Gangwani, K. K.; Lemert, R. M. Sorption and wwelling of block copolymers in the presence of supercritical fluid carbon dioxide. *J. Supercrit. Fluids* **1997**, *11*, 115–134.

(36) Kamiya, Y.; Mizoguchi, K.; Terada, K.; Fujiwara, Y.; Wang, J.-S. CO2 sorption and dilation of poly(methyl methacrylate). *Macromolecules* **1998**, *31*, 472–478.

(37) Nikitin, L. N. S.-G.; Ernest, E.; Vinokur, R. A.; Khokhlov, A. R.; Gallyamov, M. O.; Schaumburg, K. Poly(methyl methacrylate) and poly(butyl methacrylate) swelling in supercritical carbon dioxide. *Macromolecules* **2002**, *35*, 934–940.

(38) Shenoy, S. L.; Fujiwara, T.; Wynne, K. J. Quantifying plasticization and melting behavior of poly(vinylidene fluoride) in supercritical $CO_2$ utilizing a linear variable differential transformer. *Macromolecules* **2003**, *36*, 3380–3385.

(39) Royer, J. R.; DeSimone, J. M.; Khan, S. A. Carbon dioxide-induced swelling of poly (dimethylsiloxane). *Macromolecules* **1999**, *32*, 8965–8973.

(40) Shenoy, S.; Woerdeman, D.; Sebra, R.; Garach-Domech, A.; Wynne, K. Quantifying polymer swelling employing a linear variable dif-

ferential transformer (LVDT): $CO_2$ effects on styrene-butadiene-styrene triblock copolymer. *J. Macromol. Rapid Commun.* **2002**, *23*, 1130–1133.
(41) Liu, D.; Li, H.; Noon, M. S.; Tomasko, D. $CO_2$-induced PMMA Swelling and multiple thermodynamic property analysis using Sanchez-Lacombe EOS. *Macromolecules* **2005**, *38*, 4416–4424.
(42) Royer, J. R.; DeSimone, J. M.; Khan, S. A. Carbon dioxide-induced swelling of poly(dimethylsiloxane). *Macromolecules* **1999**, *32*, 8965–8973.
(43) Nikitin, L. N.; Gallyamov, M. O.; Vinokur, R. A.; Nikolaec, A. Y.; Said-Galiyev, E. E.; Khokhlov, A. R.; Jespersen, H. T.; Schaumburg, K. Swelling and impregnation of polystyrene using supercritical carbon dioxide. *J. Supercrit. Fluids* **2003**, *26*, 263–273.
(44) Rajendran, A.; Bonavoglia, B.; Forrer, N.; Storti, G.; Mazzotti, M.; Morbidelli, M. Simultaneous measurement of swelling and sorption in a supercritical CO2-poly(methyl methacrylate) system. *Ind. Eng. Chem. Res.* **2005**, *44*, 2549–2560.
(45) Bonavoglia, B.; Storti, G.; Morbidelli, M.; Rajendran, A.; Mazzotti, M. Sorption and swelling of semicrystalline polymers in supercritical $CO_2$. *J. Polym. Sci., Part B: Polym. Phys.* **2006**, *44*, 1531–1546.
(46) Keller, J. U.; Rave, H.; Staudt, R. Measurement of gas absorption in a swelling polymeric material by a combined gravimetric-dynamic method. *Macromol. Chem. Phys.* **1999**, *200*, 2269–2275.
(47) Simha, R.; Jain, R. K. Statistical thermodyanmics of blends: equation of state and phase relations. *J. Polym. Eng. Sci.* **1984**, *24*, 1284–1290.
(48) Xie, H.; Simha, R. Theory of solubility of gases in polymers. *Polym. Int.* **1997**, *44*, 348–355.
(49) Sanchez, I. C.; Lacombe, R. H. An elementary molecular theory of classical fluids. pure fluids. *J. Phys. Chem.* **1976**, *80*, 2352–2362.
(50) Sanchez, I. C.; Lacombe, R. H. Statistical thermodynamics of polymer solutions. *Macromolecules* **1978**, *11*, 1145–1156.
(51) Tait, P. G. *Physics and Chemistry of the Voyage of H.M.S. Challenger*; HMSO: London, 1888; Vol. 2, part IV.
(52) Li, Y. G. Development of a Novel Visualization and Measurement Apparatus for the PVT Behaviours of Polymer/Gas Solutions. Ph.D. Theses, MIENG University of Toronto, 2008.
(53) Li, Y. G.; Park, C. B. Effects of branching on the pressure-volume-temperature behaviors of PP/$CO_2$ solutions. *Ind. Eng. Chem. Res.* **2009**, *48*, 6633–6640.
(54) Canny, J. A computational approach to edge detection. *IEEE Trans. Pattern Anal. Machine Intell.* **1986**, *8*, 679–698.
(55) Chapra, S. C. *Applied Numerical Methods with MATLAB for Engineers and Scientists*; McGraw-Hill: Boston, 2005; Chapter 16.
(56) Dean, R. B.; Dixon, W. J. Simplified statistics for small numbers of observations. *Anal. Chem.* **1951**, *23*, 636–638.
(57) Aionicesei, E.; Skerget, M.; Knez, Z. Mathematical modelling of the solubility supercritical $CO_2$ in poly(L-lactide) and poly(D, L-lactide-co-glycolide. *J. Supercrit. Fluids* **2009**, *50*, 320–326.
(58) Hiemenz, P. C. *Polymer chemistry-The basic concept*; Marcel Dekker Inc.: NY, 1984; pp 314−315.
(59) Rodgers, P. A. Pressure-volume-temperature relationships for polymeric liquids: a review of equations of state and their characteristic parameters for 56 polymers. *J. Appl. Polym. Sci.* **1993**, *48*, 1061–1080.
(60) Machida, H.; Sato, Y.; Smith, R. L. Simple modification of the temperature dependence of the Sanchez-Lacombe equation of state. *Fluid Phase Equilib.* **2010**, accepted.
(61) Krenz, R. A.; Laursen, T.; Heidemann, R. A. The modified Sanchez-Lacombe equation of state applied to polydisperse polyethylene solutions. *Ind. Eng. Chem. Res.* **2009**, *48*, 10664–10681.
(62) Zhong, C.; Wang, W.; Lu, H. Simplified hole theory equation of state for polymer liquids. *Fluid Phase Equilib.* **1993**, *86*, 137–146.
(63) Zhong, C.; Wang, W.; Lu, H. Application of the simplified hole theory equation of state to polymer solutions and blends. *Fluid Phase Equilib.* **1994**, *102*, 173.
(64) Wang, M.; Takishima, S.; Sato, Y.; Masuoka, H. Modification of Simha-Somcynsky equation of state for small and large molecules. *Fluid Phase Equilib.* **2006**, *242*, 10–18.
(65) Wang, W.; Liu, X.; Zhong, C. Simplified hole theory equation of state for liquid polymers and solvents and their solutions. *Ind. Eng. Chem. Res.* **1997**, *36*, 2390–2398.

Received for review May 10, 2010. Accepted September 24, 2010. This project was funded by NSERC and the Consortium for Cellular and Microcellular Plastics (CCMCP). Their financial support was greatly appreciated.

JE100488V